Original Article

Investigation of subtle Lisfranc injuries using weight-bearing computed tomography

Steven M. Elicegui[1,2], Melissa R. Requist[2], Tyler J. Rogers[1], Rich J. Lisonbee[3], Yantarat Sripanich[4], Nicola Krähenbühl[4], Amy L. Lenz[3]

1. School of Medicine, University of Nevada, Reno.
2. University of Utah, Salt Lake City, USA.
3. Department of Orthopaedics, University of Utah,
4. Department of Orthopaedics, Phramongkutklao Hospital and College of Medicine, Bangkok, Thailand.
5. Department of Orthopaedics, University Hospital Basel, Basel, Switzerland.

Abstract

Introduction: Lisfranc ligamentous injuries are common yet remain a diagnostic challenge. Automated analysis of weight-bearing computed tomography (WBCT) images has been investigated to diagnose various pathologies. However, it has not been studied for Lisfranc ligament injuries. The objective of the study was to examine whether automated WBCT analysis could demonstrate diagnostic utility for these injuries.

Methods: Serial sectioning of Lisfranc complex ligaments was conducted on 24 cadaveric limbs to simulate Lisfranc injuries. WBCT images were collected at each dissection condition under three loading conditions. Images were automatically segmented, and automated measures of specific angles and distances in the midfoot were calculated using digitally reconstructed radiographs. These were analyzed using repeated measures ANOVA and paired T-tests to identify significant differences between dissections at each loading condition.

Results: Overall, minimal differences between dissection conditions were observed in automatically generated measures. Differences in axial angles of the metatarsals in severe dissections were observed, and there were fewer differences in angular measures across dissection conditions in fully loaded than unloaded conditions.

Conclusions: Automated analysis of WBCT images may indicate severe Lisfranc ligamentous injury but is insufficient to diagnose ligament injuries without full capsule disruption. This lack of injury markers may be due to the imaging conditions, automated analysis, or biomechanics of Lisfranc injuries. More alignment differences were seen under unloaded conditions, suggesting that weight-bearing imaging may not be appropriate for this injury. Overall, automated analysis shows only minimal changes in alignment measures, and additional study is necessary to improve diagnostic tools for Lisfranc injuries.

Evidence Level V; Mechanism-based reasoning.

Keywords: Lisfranc injury; Lisfranc diagnostics; Weight-bearing computed tomography; Midfoot biomechanics.

Introduction

Lisfranc injuries are the second most common athletic foot injuries due to direct high-energy trauma or low-energy forces applied to a plantar flexed foot[1-4]. Lisfranc injuries are defined as injury to the Lisfranc ligamentous complex (LLC), which consists of dorsal, interosseous, and plantar ligaments that interconnect the medial and intermediate cuneiform (C1 and C2) and first and second metatarsals (M1 and M2). The LLC is a dynamic functional unit through which multiple ligaments and joints contribute to the stability of the midfoot, and injuries to a component of this complex may destabilize the midfoot, causing differences in observed bony alignment[5-7]. The transverse arch within midfoot architecture requires a tensile load for stabilization and articulation with the forefoot. This tension is supplied by the dorsal, interosseus, and plantar ligaments, all of which connect the

C1 and M2[5,8-11]. This ligamentous support is critical for proper alignment between the midfoot and forefoot during movement. The plantar ligament has been shown to be the largest contributor to midfoot stability, and often, injuries involving this section of the complex predispose to instability that requires surgical correction[5,11,12]. Given the complexity and translational relationship of the LLC, low-energy injuries to isolated portions of this complex may not cause substantial differences in the overall structure of the midfoot.

Due to this complexity, Lisfranc injuries are a diagnostic challenge, with an estimated 20% of injuries being mis-diagnosed at initial presentation[13]. Misdiagnosis may lead to delay in treatment and potentially worse long-term outcomes[7,14,15]. The most common clinical tool for Lisfranc injury diagnosis is measuring the distance between the C1 and M2 as seen on bilateral weight-bearing radiographs[6,16-19]. However, radiographs lack interpretation of 3D joint rela-tionships, which seems compromised in Lisfranc injuries. Weight-bearing computed tomography (WBCT) is an acceptable modality to diagnose Lisfranc injuries, but 3D analysis of WBCT images is limited by computational time and personnel requirements[20,21]. Recently, automatic image segmentation and 3D measurement analysis (Bonelogic, Disior, Paragon 28, Englewood, CO) have been proposed as a solution to these challenges and have been investigated in various foot and ankle pathologies. This analysis has not been studied for Lisfranc injury diagnosis, and beyond its utility as a diagnostic tool, it may provide insight into the mechanical function of the LLC ligamentous components in stabilizing the midfoot.

The objective of this study is to examine differences in automatically generated measurements in simulated ca-daveric Lisfranc injuries to determine the feasibility of this analysis as an adjunct diagnostic tool.

METHODS
Specimen preparation

After approval from the Institutional Review Board, 24 through-knee cadaveric specimens (12 matched pairs) were obtained for the study. Inclusion criteria included male cadavers ages 18 to 65 years with a body mass index (BMI) of less than 30. Exclusion criteria disqualified individuals with previous foot and ankle injuries, neoplastic bone involvement, or surgeries to the lower extremity. An external fixator consisting of an Ilizarov apparatus using four 1.5 mm Kirschner wires held in a radiolucent frame was attached to each specimen to keep them in a plantigrade position[22,23].

Serial dissections

To simulate reproducible isolated Lisfranc ligamentous injuries, a stepwise serial dissection of the Lisfranc complex was carefully performed by a board-certified fellowship-trained orthopedic surgeon. The process began with a dorsal incision to visualize and confirm the intact Lisfranc complex. The serial dissection occurred in the following

order: dorsal ligament connecting C1 to M2 (Condition D1), interosseous ligament connecting C1 to M2 (Condition D2), and plantar ligament connecting C1 to M2 and M3 (Condition D3). The initial three conditions simulated individualized interruption of the three primary stabilizing components of the Lisfranc complex[10]. After serial dissection of these three main components, the capsules of the first and second tarsometatarsal joints (TMT1 and TMT2, respectively) and the medial-middle inter-cuneiform ligament were dissected in a randomized order (Condition CD). This condition involved the complete dissection of midfoot Lisfranc joint soft tissue support structures and was used for statistical comparison of a fully dissected ligament complex, even though it is not representative of a typical injury mechanism.

Image acquisition

Before dissection and following each dissection step (conditions D1-CD), WBCT scans were acquired under three weight-bearing (loading) conditions. The load was applied using weights placed on top of the external fixator. The three loading conditions were unloaded (0 kg), partially loaded (40 kg), and fully loaded (90 kg). The load amounts were chosen to provide a reasonable estimation of body weight while conserving the specimen for serial dissection and imaging. WBCT images were collected using a pedCAT (CurveBeam LLC; medium view, 0.3 mm slice thickness, 0.3 mm slice interval, kVp 120, mAs 22 – 62), totaling 360 WBCT images.

Image segmentation and analysis

After WBCT images were obtained with all dissection and loading conditions, images were segmented automatically from manually labeled seed points on each bone (Bonelogic, DISIOR, Paragon 28, Englewood, CO). 3D models were exported from these segmentations and manually inspected for accuracy (Mimics, Materialize, Leuven, Belgium). Segmen-ted images were used to generate digitally reconstructed radiographs and automatically calculate specific angle and distance measurements in the midfoot (Bonelogic, DISIOR, Paragon 28, Englewood, CO). The nine midfoot measurements calculated and analyzed were the M1-M2 intermetatarsal angle in the axial and sagittal planes, TMT1 and TMT2 angles in the axial and sagittal planes, TMT1 minimum joint space, M1 torsion, and M1 internal rotation (Figure 1).

Data analysis

A repeated measures ANOVA was used to examine diffe-rences between dissection conditions for each outcome variable at each loading condition. The repeated measures ANOVA was chosen due to a stepwise progression through dissection conditions, where there are more dissected ligaments at each subsequent condition. By comparing each measure to earlier measures of the same specimen, the repeated measures ANOVA normalizes data and accounts for within-subject variability to provide a more accurate data analysis than a traditional ANOVA[24]. ANOVA analysis
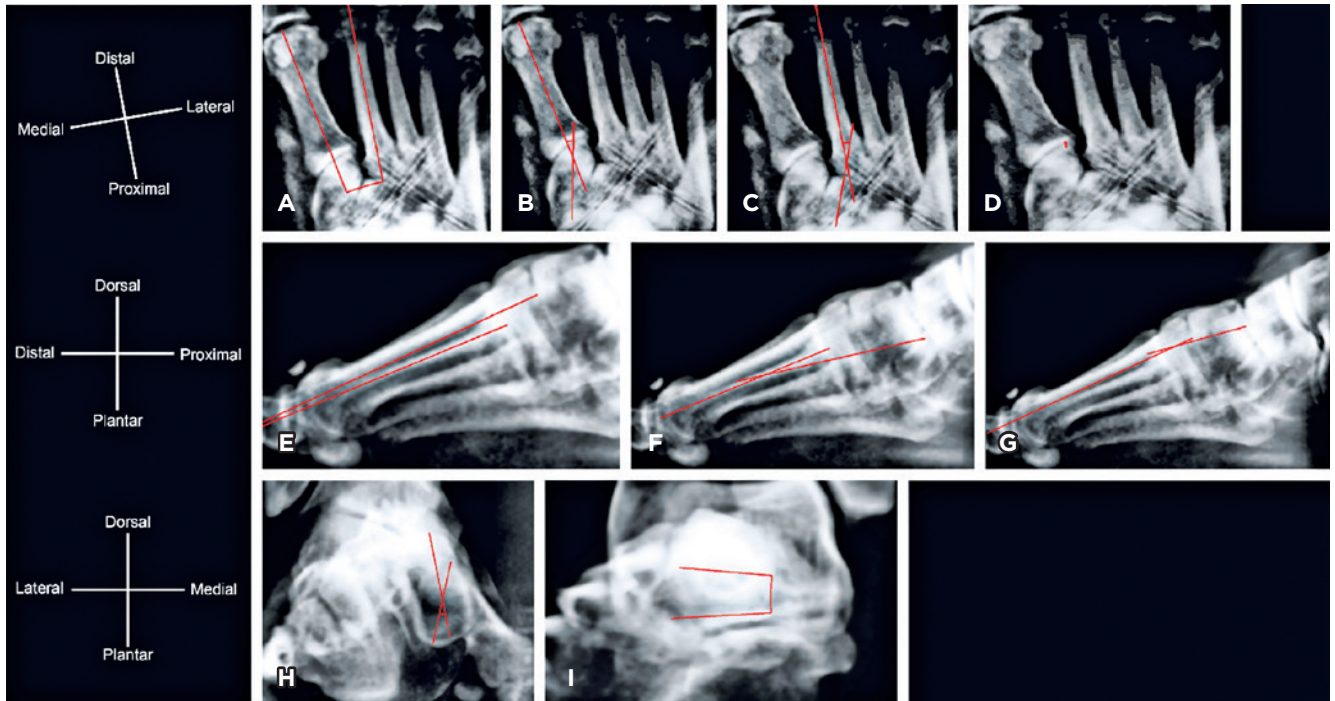
Figure 1. Digitally reconstructed radiographs from DISIOR showing the automatically calculated measures of (A) axial plane angle between the first and second metatarsal, (B) axial plane angle between the medial cuneiform and first metatarsal (first tarsometatarsal joint), (C) axial plane angle between the intermediate cuneiform and second metatarsal (second tarsometatarsal joint), (D) minimum joint space in the first tarsometatarsal joint, (E) sagittal plane angle between the first and second metatarsals, (F) sagittal plane angle of the first tarsometatarsal joint, (G) sagittal plane angle of the second tarsometatarsal joint, (H) first metatarsal torsion, and (I) first metatarsal internal rotation.

used a significance value of $\alpha = 0.05$. Following the repeated measures ANOVA, all combinations of outcome variables and loading conditions that showed a significant difference between dissection conditions were further analyzed using paired t-tests as a post-hoc analysis to compare each combination of dissection conditions. This step provides a detailed understanding of which injury types could be differentiated using each output condition. While existing studies using DISIOR typically use a significance value of 0.05[25,26], these post-hoc paired t-tests used a significance value of $\alpha = 0.01$ due to the high number of comparisons made in this analysis. This does not reflect a mathematical correction, as a Bonferroni correction is too conservative for this use, but it does reduce the likelihood of false significance findings[27]. Using paired t-test for this post-hoc analysis retains the within-subject comparison of the repeated measures ANOVA and determines at what points the differences are significant, not just which outcomes had significant change at some point in the dissection. This effectively tests not just the mechanical changes to the joint structure but also the severity of injury needed to identify the injury using these methods. Statistical tests were conducted using raw data because both the repeated measures ANOVA and paired

t-tests intrinsically account for within-subject variability, but data was normalized for graphical representation to illustrate the changes between conditions better.

Results

Repeated measures ANOVA showed significant differences between dissection conditions for the TMT1 axial angle in all three loading conditions, the TMT2 axial angle in all three loading conditions, and both the intermetatarsal axial angle and the M1 sagittal angle at the unloaded condition only. All other outcome variables did not show statistically significant differences among dissection conditions at any loading condition. The mean and standard deviation for all outcome measures at each dissection and loading condition are given in Table 1, and all p-values for repeated measure ANOVA tests for differences between any two dissection conditions at each loading condition are given in Table 2.

Post-hoc analysis of the intermetatarsal sagittal angle in the unloaded condition showed a significant difference between the complete dissection condition (CD) and each of the other dissection conditions (D1, D2, and D3) but not the undissected condition (UND). The intermetatarsal angle

Table 1. Mean and standard deviation (SD) for each outcome measure under each combination of loading and dissection conditions.

		M1-M2 Axial		M1-M2 Sagittal		TMT1 Sagittal		TMT2 Sagittal		TMT1 Axial		TMT2 Axial		M1 Torsion		M1 Rotation		TMT1 Min Joint Space	
		Mean	SD	Mean	SD	Mean	SD	Mean	SD	Mean	SD	Mean	SD	Mean	SD	Mean	SD	Mean	SD
Unloaded	UND	10.12	2.90	1.27	2.40	9.12	2.84	6.08	3.18	-24.85	3.09	-23.89	4.96	17.65	5.30	-3.42	7.95	1.12	0.10
	D1	10.19	2.77	1.26	2.50	9.31	2.92	6.24	2.79	-24.79	3.02	-23.72	4.73	17.53	6.54	-2.38	5.72	1.14	0.16
	D2	10.08	2.88	1.01	2.60	10.08	3.69	6.83	2.91	-24.51	3.04	-23.63	4.86	17.74	7.62	-2.97	7.81	1.17	0.13
	D3	10.23	2.80	1.16	2.53	9.80	2.46	6.71	2.91	-24.30	3.69	-23.18	5.02	18.38	7.47	-2.19	6.62	1.15	0.10
	CD	9.82	2.48	2.15	2.41	9.01	2.82	6.81	2.70	-23.04	4.25	-22.76	5.00	17.39	12.37	-2.07	12.89	1.20	0.11
Partially Loaded	UND	10.49	3.00	1.67	2.35	9.12	2.75	6.44	2.85	-24.62	3.19	-23.42	4.94	17.19	7.24	-2.53	8.98	1.12	0.13
	D1	10.59	2.95	1.74	2.38	9.12	2.71	6.59	2.91	-24.67	3.05	-23.30	4.95	18.20	8.13	-4.57	12.50	1.15	0.13
	D2	10.71	2.98	1.73	2.41	9.46	2.93	6.91	2.62	-24.34	3.22	-23.03	4.91	17.96	7.35	-1.08	7.98	1.17	0.08
	D3	10.74	2.81	1.73	2.34	9.60	2.57	6.92	2.73	-24.10	3.58	-22.92	5.00	18.21	7.11	-3.30	8.09	1.15	0.09
	CD	10.62	2.63	1.96	2.19	9.28	3.06	6.71	2.70	-23.82	4.39	-22.74	5.23	19.43	8.82	-4.22	6.56	1.16	0.08
Fully Loaded	UND	10.73	2.96	1.92	2.33	8.96	2.78	6.63	2.79	-24.80	3.31	-23.25	5.06	17.41	5.84	-2.91	5.22	1.13	0.13
	D1	10.81	2.90	1.76	2.33	9.27	2.81	6.58	2.98	-24.63	3.28	-23.18	4.96	17.47	6.47	-2.46	7.86	1.12	0.13
	D2	10.80	2.98	1.71	2.40	9.48	2.99	6.97	2.47	-24.26	3.48	-22.81	5.08	18.10	7.99	-3.79	8.58	1.11	0.15
	D3	10.84	2.87	1.72	2.41	9.57	2.93	6.91	2.76	-23.95	3.74	-22.67	5.17	17.21	6.03	-2.04	7.99	1.10	0.23
	CD	10.51	2.68	2.02	2.31	9.26	3.35	6.83	2.76	-23.74	4.95	-22.64	5.39	17.37	12.63	-2.20	12.46	1.14	0.10

C1: Medial cuneiform; C2: Intermediate cuneiform; M1: First metatarsal; M2: Second metatarsal; TMT1: First tarsometatarsal; TMT2: Second tarsometatarsal.
Serial dissection conditions consist of undissected (UND), dissection of C1-M2 dorsal ligament (D1), dissection of C1-M2 interosseous ligament (D2), dissection of C1-M2 and M3 plantar ligament (D3), and complete dissection of the TMT1 and TMT2 joint capsules and the medial-middle inter-cuneiform ligament (CD).

Table 2. P-values for repeated measures ANOVA of each outcome value and loading condition across the four dissection conditions. Tests showing statistical significance are in bold and represent any outcome measure under a specific loading condition with a significant difference between at least two of the five dissection conditions.

Outcome Measure	Unloaded	Partially Loaded	Fully Loaded
Intermetatarsal axial angle	0.170	0.404	0.347
Intermetatarsal sagittal angle	**0.002**	0.205	0.352
TMT1 axial angle	**< 0.001**	**0.034**	**0.044**
TMT1 sagittal angle	**0.035**	0.136	0.225
TMT2 axial angle	**< 0.001**	**0.010**	**0.024**
TMT2 sagittal angle	**0.013**	0.184	0.307
TMT1 rotation	0.837	0.269	0.762
TMT1 torsion	0.795	0.283	0.853
TMT1 minimum joint space	0.058	0.361	0.684

TMT1: First tarsometatarsal; TMT2: Second tarsometatarsal.

value was significantly greater in condition CD than in the other three dissection conditions. The TMT1 sagittal angle in the unloaded condition showed a significant difference between the UND and dissection D3, where the angle was greater in dissection D3 than in the UND. P-values for each of these comparisons are given in Table 3.

Post-hoc analysis of the TMT1 axial angle at the unloaded condition yielded a significantly increased angle axial angle in dissection condition CD than in each other dissection condition, including the UND. However, there were no significant differences between dissection condition CD and any other dissection condition in the partially and fully loaded conditions. In the partially loaded condition, the angle was significantly greater under dissection condition D3 than condition D1. In the fully loaded condition, conditions D2 and D3 had significantly greater angle measurements than condition D1. P-values for the TMT1 post-hoc tests of all three loading conditions are given in Table 4.

Post-hoc analysis of the TMT2 axial angle in the unloaded condition revealed significantly greater angle measurements in dissections D3 and D4 than in the UND or dissection D1. The significant increase in axial angle between the UND and conditions D3 and D4 was also present in the partially loaded condition. There were significant differences between dissection condition D3 and the UND and condition D1 in the fully loaded state. P-values for the TMT2 post-hoc tests in all three loading conditions are given in Table 4.

Discussion

Given the difficulties in subtle Lisfranc injury diagnosis and the long-term implications of missed injuries, an improvement in diagnostic methods is needed. Automated analysis pipelines may overcome the logistical barrier preventing 3D image analysis, but thus far, they are not effective as adjunctive diagnostic tools. This study investigated auto-matically generated measures of 3D alignment as indicators of simulated presence and severity of Lisfranc injury. Several individual joint angles within the midfoot showed significant differences with simulated Lisfranc injuries, but

the change in these outcome measures was minimal. Most of the significant differences were seen in comparisons that included the complete dissection (CD) condition, and no outcome measures showed significant differences between all sequential ligament dissections. While several outcome measures showed significant differences between CD and UND or CD and early dissection conditions (D1 or D2), these differences are not clinically relevant because the CD condition is not representative of a known injury mechanism.

Table 3. Post-hoc analysis of the intermetatarsal sagittal angle, first tarsometatarsal sagittal angle, and second tarsometatarsal sagittal angle in the unloaded condition showing p-values from paired t-tests comparing each pair of dissection conditions. Tests showing statistical significance are in bold.

Comparison	Intermetatarsal sagittal angle	TMT1 sagittal angle	TMT2 sagittal angle
UND – D1	0.878	0.372	0.485
UND – D2	0.104	0.024	**0.003**
UND – D3	0.475	**0.003**	0.015
UND – CD	0.015	0.786	0.024
D1 – D2	0.136	0.075	0.020
D1 – D3	0.432	0.019	0.036
D1 – CD	**0.008**	0.435	0.026
D2 – D3	0.413	0.519	0.915
D2 – CD	**0.002**	0.037	0.770
D3 – CD	**0.002**	0.042	0.684

C1: Medial cuneiform; C2: Intermediate cuneiform; M1: First metatarsal; M2: Second metatarsal; TMT1: First tarsometatarsal; TMT2: Second tarsometatarsal.
Serial dissection conditions consist of undissected (UND), dissection of C1-M2 dorsal ligament (D1), dissection of C1-M2 interosseous ligament (D2), dissection of C1-M2 and M3 plantar ligament (D3), and complete dissection of the TMT1 and TMT2 joint capsules and the medial-middle inter--cuneiform ligament (CD).

No outcome measures showed significant differences between UND and D1, and only TMT2 axial and sagittal angles showed significant differences between UND and D2. However, neither measure showed significance between D2 and any other dissection condition. TMT1 sagittal and TMT2 axial angles showed significant differences between UND and D3, and the TMT2 axial angle additionally had a significant difference between D1 and D3 with a trend of decreasing magnitude of this angle measure with progressive dissection conditions while unloaded. More significant differences were observed under unloaded conditions than in partially or fully loaded conditions. This contradicts the belief that weight-bearing imaging improves diagnostic accuracy and suggests that load may stabilize the midfoot and mask subtle structural changes.

The poor ability of this analysis to distinguish between simulated subtle injury conditions may be caused by many factors. As mentioned, weight-bearing imaging may not be ideal for identifying Lisfranc injuries. The outcome measures tested in this study were chosen based on ease of use, as they are the automatically generated midfoot measures from this software with the assumption that manually calculated 3D measures would not be clinically transferrable due to the time and skill needed to complete a manual analysis. However, these measures may not be the most effective for identifying the alignment change caused by subtle Lisfranc injuries. Further, bony alignment may be a poor measure of Lisfranc complex stability under any imaging modality or analysis technique. The midfoot is a highly biomechanically stabilized joint, with redundancy in stabilization through the many articulations and ligaments in the Lisfranc complex and surrounding areas of the foot[8]. Without substantial change in bony alignment, the challenges of Lisfranc diagnosis from radiographs would not be remedied by computed

Table 4. Post-hoc analysis of the first and second tarsometatarsal axial angles at each loading condition showing p-values from paired t-tests comparing each pair of dissection conditions. UND represents the undissected condition, and D1, D2, D3, and CD represent the serial dissection conditions. Tests showing statistical significance are in bold.

Comparison	TMT1 Axial Angle			TMT2 Axial Angle		
	Unloaded	Partially Loaded	Fully Loaded	Unloaded	Partially Loaded	Fully Loaded
UND - D1	0.619	0.043	0.428	0.095	0.257	0.517
UND - D2	0.049	0.033	0.025	0.189	0.017	**0.002**
UND – D3	0.087	0.014	0.030	**0.001**	**0.004**	**0.001**
UND – CD	**< 0.001**	0.036	0.057	**< 0.001**	**0.003**	0.024
D1 – D2	0.108	0.016	**0.006**	0.640	0.078	0.016
D1 – D3	0.122	**0.009**	**0.004**	**0.006**	0.021	**0.002**
D1 – CD	**< 0.001**	0.036	0.055	**0.003**	0.028	0.063
D2 – D3	0.491	0.191	0.127	0.054	0.533	0.419
D2 – CD	**0.002**	0.162	0.231	0.010	0.268	0.565
D3 - CD	**0.001**	0.338	0.590	0.076	0.335	0.885

C1: Medial cuneiform; C2: Intermediate cuneiform; M1: First metatarsal; M2: Second metatarsal; TMT1: First tarsometatarsal; TMT2: Second tarsometatarsal.
Serial dissection conditions consist of undissected (UND), dissection of C1-M2 dorsal ligament (D1), dissection of C1-M2 interosseous ligament (D2), dissection of C1-M2 and M3 plantar ligament (D3), and complete dissection of the TMT1 and TMT2 joint capsules and the medial-middle inter-cuneiform ligament (CD).

tomography imaging. More accurate diagnostic imaging may require soft tissue imaging modalities.

Previous research has demonstrated that the plantar ligament of the LLC is important in providing midfoot stability and that disruption of this ligament likely contributes to the instability of the midfoot that necessitates surgical fixation[5,11,28]. This importance of the plantar ligament is supported by our data showing significant changes from the UND in TMT1 sagittal and TMT2 axial angles only in conditions where the plantar ligament had been dissected (dissection conditions D3 and D4). While these data suggest that the TMT1 sagittal and TMT2 axial angles may be relevant for diagnosing more severe Lisfranc injuries, the lack of difference to other dissection conditions is concerning because the angles may not be different enough for identification without having an uninjured control for comparison. Further, the more severe Lisfranc injuries are less likely to be missed using current diagnostics than subtle injuries, so the analysis may not be worthwhile if it can only identify severe injuries that may be seen using simpler diagnostic tools.

Weight-bearing imaging is commonly believed to be superior to non-weight-bearing imaging in the foot and ankle[8,29,30]. However, these data contradict this theory as there were a greater number of significant differences in outcome measures under unloaded conditions than under partially or fully loaded conditions, which may be due to the ability of the midfoot to distribute static load across bone rather than soft tissue to ensure proper alignment across dynamic movement. This indicates that non-weight-bearing imaging may have a role in investigating Lisfranc injury diagnostics.

While this study offers insight into the pathological changes in midfoot angles in Lisfranc Injuries, several limitations exist. The automatic analysis software used for this study has not been robustly validated. Studies have shown promising reliability between automatically generated and manually calculated measurements, but the image segmentations used to calculate these measures have not been validated[31-33]. Additionally, some potentially valuable measures, such as rotation of the TMT2 joint, were not available. However, the objective of this study was to observe if the automatic analysis, even with unknown intrinsic error, would prove to be a useful diagnostic tool. The comparisons made in this analysis are to undissected conditions of the same specimen and thus normalize for much of the population variation in midfoot alignment, but comparisons of these actual measures to population means may not be appropriate. This study did not investigate using an uninjured contralateral limb as a control for comparison, but that may be a way to alleviate this concern. As previously mentioned, the complete dissection condition (CD) did not represent a known injury mechanism, as Lisfranc injuries involving both the inter-cuneiform ligament and TMT capsule are uncommon[12,34]. While it is a beneficial statistical comparison for this analysis, this dissection condition has limited application for understanding clinical presentation. Cadaveric models with simulated injuries are limited by their lack of active muscle contractions that may contribute to detecting Lisfranc injuries and by the absence of comorbid foot deformity or additional injury that may complicate the findings for a subtle Lisfranc injury.

Conclusion

Automatic analysis of 3D imaging is an exciting advancement that may allow for more detailed clinical analysis of foot alignment for subtle injury diagnosis. However, these data do not support using this technology as an adjunct diagnostic tool for Lisfranc injuries. This may be due to the outcome measures included in this analysis, the potential masking of injury under weight-bearing, or the mechanism of the injury itself. These data support further investigation of the role of weight-bearing vs non-weight-bearing imaging in midfoot injuries and the potential utilization of non-bony imaging methods to improve Lisfranc injury diagnosis.

References

1. Stødle AH, Hvaal KH, Enger M, Brøgger H, Madsen JE, Ellingsen Husebye E. Lisfranc injuries: Incidence, mechanisms of injury and predictors of instability. Foot Ankle Surg. 2020;26(5):535-40.

2. Kalia V, Fishman EK, Carrino JA, Fayad LM. Epidemiology, imaging, and treatment of Lisfranc fracture-dislocations revisited. Skeletal Radiol. 2012;41(2):129-36.

3. Murphy N, Olney D. Lisfranc joint injuries: trauma mechanisms and associated injuries. J Trauma. 1994;36(3):464-5.

4. Hill JF, Heyworth BE, Lierhaus A, Kocher MS, Mahan ST. Lisfranc injuries in children and adolescents. J Pediatr Orthop B. 2017;26(2):159-63.

5. Raikin SM, Elias I, Dheer S, Besser MP, Morrison WB, Zoga AC. Prediction of midfoot instability in the subtle Lisfranc injury. Comparison of magnetic resonance imaging with intraoperative findings. J Bone Joint Surg Am. 2009;91(4):892-9.

6. Sripanich Y, Weinberg M, Krahenbuhl N, Rungprai C, Saltzman CL, Barg A. Change in the First Cuneiform-Second Metatarsal Distance After Simulated Ligamentous Lisfranc Injury Evaluated by Weightbearing CT Scans. Foot Ankle Int. 2020;41(11):1432-41.

7. Ingall EM, Raduan F, Kwon JY. A novel flexible fixation technnique for Lisfranc injuries: clinical outcomes and radiographic follow-up. Journal of the Foot and Ankle. 2023;17(3):183-90.

8. Garriguez-Perez D, Puerto-Vazquez M, Tome Delgado JL, Galeote E, Marco F. Impact of the Subtle Lisfranc Injury on Foot Structure and Function. Foot Ankle Int. 2021;42(10):1303-10.

9. Johnson A, Hill K, Ward J, Ficke J. Anatomy of the lisfranc ligament. Foot Ankle Spec. 2008;1(1):19-23.

10. Chen J, Sagoo N, Panchbhavi VK. The Lisfranc Injury: A Literature Review of Anatomy, Etiology, Evaluation, and Management. Foot Ankle Spec. 2021;14(5):458-67.

11. Haraguchi N, Ota K, Ozeki T, Nishizaka S. Anatomical Pathology of Subtle Lisfranc Injury. Sci Rep. 2019;9(1):14831.

12. Siddiqui NA, Galizia MS, Almusa E, Omar IM. Evaluation of the tarsometatarsal joint using conventional radiography, CT, and MR imaging. Radiographics. 2014;34(2):514-31.

13. Sherief TI, Mucci B, Greiss M. Lisfranc injury: how frequently does it get missed? And how can we improve? Injury. 2007;38(7):856-60.

14. Singh A, Lokikere N, Saraogi A, Unnikrishnan PN, Davenport J. Missed Lisfranc injuries-surgical vs conservative treatment. Ir J Med Sci. 2021;190(2):653-6.

15. Tarczyńska M, Gawęda K, Dajewski Z, Kowalska E, Gągała J. Comparison of treatment results of acute and late injuries of the lisfranc joint. Acta Ortop Bras. 2013;21(6):344-3446.

16. Aronow MS. Treatment of the missed Lisfranc injury. Foot Ankle Clin. 2006;11(1):127-42, ix.

17. Hardcastle PH, Reschauer R, Kutscha-Lissberg E, Schoffmann W. Injuries to the tarsometatarsal joint. Incidence, classification and treatment. J Bone Joint Surg Br. 1982;64(3):349-56.

18. Coss HS, Manos RE, Buoncristiani A, Mills WJ. Abduction stress and AP weightbearing radiography of purely ligamentous injury in the tarsometatarsal joint. Foot Ankle Int. 1998;19(8):537-41.

19. Llopis E, Carrascoso J, Iriarte I, Serrano MDP, Cerezal L. Lisfranc Injury Imaging and Surgical Management. Seminars in Musculoskeletal Radiology. 2016;20(2):139-53.

20. Bhimani R, Sornsakrin P, Ashkani-Esfahani S, Lubberts B, Guss D, De Cesar Netto C, et al. Using area and volume measurement via weightbearing CT to detect Lisfranc instability. J Orthop Res. 2021;39(11):2497-505.

21. Ota T, Nagura T, Kokubo T, Kitashiro M, Ogihara N, Takeshima K, et al. Etiological factors in hallux valgus, a three-dimensional analysis of the first metatarsal. J Foot Ankle Res. 2017;10:43.

22. Burssens A, Krahenbuhl N, Lenz AL, Howell K, Zhang C, Sripanich Y, et al. Interaction of loading and ligament injuries in subtalar joint instability quantified by 3D weightbearing computed tomography. J Orthop Res. 2022;40(4):933-44.

23. Burssens A, Krähenbühl N, Weinberg MM, Lenz AL, Saltzman CL, Barg A. Comparison of External Torque to Axial Loading in Detecting 3-Dimensional Displacement of Syndesmotic Ankle Injuries. Foot Ankle Int. 2020;41(10):1256-68.

24. Park E, Cho M, Ki CS. Correct use of repeated measures analysis of variance. Korean J Lab Med. 2009;29(1):1-9.

25. An T, Haupt E, Michalski M, Salo J, Pfeffer G. Cavovarus With a Twist: Midfoot Coronal and Axial Plane Rotational Deformity in Charcot-Marie-Tooth Disease. Foot Ankle Int. 2022;43(5):676-82.

26. Michalski MP, An TW, Haupt ET, Yeshoua B, Salo J, Pfeffer G. Abnormal Bone Morphology in Charcot-Marie-Tooth Disease. Foot Ankle Int. 2022;43(4):576-81.

27. Feise RJ. Do multiple outcome measures require p-value adjustment? BMC Med Res Methodol. 2002;2:8.

28. Suzuki Y, Edama M, Kaneko F, Ikezu M, Matsuzawa K, Hirabayashi R, Kageyama I. Morphological characteristics of the Lisfranc ligament. J Foot Ankle Res. 2020;13(1):46.

29. Gupta RT, Wadhwa RP, Learch TJ, Herwick SM. Lisfranc injury: imaging findings for this important but often-missed diagnosis. Curr Probl Diagn Radiol. 2008;37(3):115-26.

30. De Bruijn J, Hagemeijer NC, Rikken QGH, Husseini JS, Saengsin J, Kerkhoffs G, et al. Lisfranc injury: Refined diagnostic methodology using weightbearing and non-weightbearing radiographs. Injury. 2022;53(6):2318-25.

31. Krahenbuhl N, Kvarda P, Susdorf R, Burssens A, Ruiz R, Barg A, Hintermann B. Assessment of Progressive Collapsing Foot Deformity Using Semiautomated 3D Measurements Derived From Weightbearing CT Scans. Foot Ankle Int. 2022;43(3):363-70.

32. Ortolani M, Leardini A, Pavani C, Scicolone S, Girolami M, Bevoni R, et al. Angular and linear measurements of adult flexible flatfoot via weight-bearing CT scans and 3D bone reconstruction tools. Sci Rep. 2021;11(1):16139.

33. Kvarda P, Heisler L, Krahenbuhl N, Steiner CS, Ruiz R, Susdorf R, et al. 3D Assessment in Posttraumatic Ankle Osteoarthritis. Foot Ankle Int. 2021;42(2):200-14.

34. Kitsukawa K, Hirano T, Niki H, Tachizawa N, Mimura H. The Diagnostic Accuracy of MRI to Evaluate Acute Lisfranc Joint Injuries: Comparison With Direct Operative Observations. Foot Ankle Orthop. 2022;7(1):24730114211069080.